HHS Public Access

Author manuscript

DNA Repair (Amst). Author manuscript; available in PMC 2020 August 01.

Published in final edited form as:

DNA Repair (Amst). 2019 August ; 80: 1–7. doi:10.1016/j.dnarep.2019.06.002.

Quantitative Analysis of ATM Phosphorylation in Lymphocytes

Christopher J. Bakkenist, Ph.D.[1,2], **R. Kenneth Czambel, B.S.**[3], **Yan Lin, Ph.D.**[4], **Nathan A. Yates, Ph.D.**[5,6], **Xuemei Zeng, Ph.D.**[6], **Jeffery Shogan, B.S.**[1], **John C. Schmitz, Ph.D.**[3]

[1]Department of, Radiation Oncology, University of Pittsburgh School of Medicine, 5117 Centre Avenue, Pittsburgh, PA 15213-1863

[2]Department of Pharmacology and Chemical Biology, University of Pittsburgh School of Medicine, 5117 Centre Avenue, Pittsburgh, PA 15213-1863

[3]Department of Medicine, University of Pittsburgh School of Medicine, 5117 Centre Avenue, Pittsburgh, PA 15213-1863

[4]Departments of Biostatistics, University of Pittsburgh School of Medicine, 5117 Centre Avenue, Pittsburgh, PA 15213-1863

[5]Departments of Cell Biology, University of Pittsburgh School of Medicine, 5117 Centre Avenue, Pittsburgh, PA 15213-1863

[6]Biomedical Mass Spectrometry Center, University of Pittsburgh School of Medicine, 5117 Centre Avenue, Pittsburgh, PA 15213-1863

Abstract

Since many anticancer therapies target DNA and DNA damage response pathways, biomarkers of DNA damage endpoints may prove valuable in basic and clinical cancer research. Ataxia telangiectasia-mutated (ATM) kinase is the principal regulator of cellular responses to DNA double-strand breaks (DSBs). In humans, ATM autophosphorylation at serine 1981 (p-S1981) is an immediate molecular response to nascent DSBs and ionizing radiation (IR). Here we describe the analytical characteristics and fit-for-purpose validation of a quantitative dual-labeled immunoblot that simultaneously measures p-S1981-ATM and pan-ATM in human peripheral blood mononuclear cells (PBMCs) following ex vivo exposure to 2 Gy IR, facilitating the calculation of %p-ATM. To validate our assay, we isolated PBMCs from 41 volunteers. We report that the median basal level of p-S1981-ATM and pan-ATM was 2.4 and 49.5 ng/10^7 PBMCs, respectively, resulting in %p-ATM of 4%. Following exposure of PBMCs to 2 Gy IR, p-S1981-ATM levels increased 12-fold to 29.8 ng/10^7 PBMCs resulting in %p-ATM of 63%. Interestingly, we show that PBMCs from women have a 2.6-fold greater median p-S1981-ATM level following IR exposure than men (44.4 versus 16.9 ng/10^7 cells; $p < 0.01$). This results in a significantly greater %p-ATM for women (68% versus 49%; $p < 0.01$). Our rigorous description of the

Corresponding author: John C. Schmitz, Ph.D., Ph: 412-864-7743, schmitzjc@upmc.edu.

Conflicts of Interest: Authors have no conflicts of interest to disclose.

analytical characteristics and reproducibility of phosphoprotein immunoblotting, along with our finding that the ATM DNA damage response is greater in women, has far reaching implications for biomedical researchers.

Keywords

Ataxia telangiectasia-mutated kinase; DNA damage response; biomarker; PBMC; sex as a biological variable

1. Introduction

Failure of many cancer therapies in late clinical trials may be attributed, in part, to a lack of pharmacodynamic (PD) biomarker incorporation in early clinical development. The use of PD biomarkers allows clinical outcome in patients to be evaluable in terms of both biological processes and clinical endpoint. Accordingly, a “pharmacological audit trail” would allow trial design to be modified and/or treatments repurposed as their efficacy is assessed in patients [1]. Since genotoxic chemotherapies target DNA, biomarkers that identify DNA damage signaling may prove particularly useful [2]. It has been reported that DNA damage-induced ATM (ataxia telangiectasia-mutated) kinase autophosphorylation on serine-1981 (p-S1981-ATM) is a plausible biomarker of DNA double-stand breaks (DSBs) [3–6].

Comprehensive validation and clinical qualification are essential prior to the introduction of a biomarker. Analytical validation encompasses the assay performance characteristics and optimization of assay conditions to maximize accuracy and minimize imprecision. In contrast, clinical qualification is the evidentiary process of connecting biomarkers with biological processes and clinical endpoints [7]. Furthermore, “fit-for-purpose” validation is essential in the specimens for which the biomarker is intended [8].

Quasi-quantitative immunoblots are often used for analysis of protein post-translational modifications [9, 10]. Previously we described a novel quasi-quantitative multiplexed immunoblot method that simultaneously measures ATM and histone H2AX phosphorylation in human peripheral blood mononuclear cells (PBMCs) [5]. Here, we report the fit-for-purpose validation of an immunoblot assay that uses human recombinant ATM (rATM) calibration standard. Using this quantitative immunoblot to analyze irradiated PBMCs collected from normal volunteers, we report the first quantitation of p-S1981-ATM in human tissues and reveal that the ATM-mediated DNA damage response is greater in women.

2. Materials and Methods

2.1. Subjects

Human studies were approved by the UPMC Health System/University of Pittsburgh Institutional Review Board. Written informed consent was obtained from each volunteer.

2.2. Materials

Recombinant human ATM kinase (rATM) was purchased from Eurofins Pharma Bioanalytics Services. rATM was re-aliquoted into single-use tubes (50 ng) and refrozen. Purified peptides SLAFEEGSQSTTISSLSEK(S1981) and SLAFEEG-pS-QSTTISSLSEK(p-S1981) were obtained from Anaspec and quantified by HPLC and BCA assay. Antibodies: phospho-S1981-ATM (clone EP1890Y, cat#:ab81292, Abeam); pan-ATM (clone 2C1, cat#GTX70103, GeneTex); phosphoserine-139 histone H2AX (clone 20E3, cat#9718, Cell Signaling); histone H2AX (clone 322105, cat#MAB3406, R&D Systems); IRDye-800CW (cat#926-32211, LI-COR Biotechnology-US); IRDye-680RD (cat#926-68070, LI-COR). The ViaStain™ AOPI Staining Solution and Cellometer slides were purchased from Nexcelom Bioscience.

2.3. Lysis Buffer Formulation

1× DTT-modified Laemmli buffer: 69 mM Tris-HCI pH 6.8, 100 mM DTT, 11% glycerol, 1% LDS, 0.005% bromophenol blue, with 1× protease/phosphatase inhibitor cocktails added before use (prepared from 4× Laemmli Buffer (cat#1610747, Bio-Rad)).

2.4. Identification of rATM peptides with unmodified S1981 and phosphorylated p-S1981

To identify the free-acid and phosphorylated tryptic peptides from rATM, a Coomassie-blue stained band containing ~3.0 μg of rATM was trypsin-digested and analyzed by LC-MS/MS as described previously [11]. The gel band was destained with 50% acetonitrile/25 mM ammonium bicarbonate. Reduction and alkylation were achieved by incubating the gel in 10 mM DTT at 56°C for 1 hour followed by 1 hour incubation in the dark with the addition of 55 mM iodoacetamide (IAA). Trypsin (20 ng/ul) was added and digestion proceeded overnight at 37°C. Peptides were extracted with 70% acetonitrile/5% formic acid, vacuum-dried, reconstituted in 0.1% formic acid and analyzed by a Waters NanoAcquity HPLC interfaced to a MS (LTQ-Orbitrap Velos). The separation was performed on a PicoChip™ Reprosil C18 column (New Objective Inc) using a binary reverse-phase gradient (flow rate, 300 nL/min). The MS was operated in a data-dependent mode, with high-resolution full MS spectra performed at 60000 FWHM resolution, and data-dependent acquisition was used to collect tandem mass spectra for the 13 most abundant ions detected. MS/MS spectra were searched against human protein database using MASCOT search engine (Version 2.4.0, Matrix Science Ltd). The mass tolerance was set at 20 ppm for the precursor ions and 0.8 Da for product ions using tryptic enzyme specificity with two missed cleavages allowed. Carboxy-aminomethylation of cysteine residues was set as a static modification. Oxidation of methionine residues and phosphorylation of serine, threonine and tyrosine residues were set as variable modification.

2.5. Measurement of the percentage of rATM phosphorylated at S1981

High-resolution precursor ion chromatograms (MS1) at m/z=1000.99(S1981) and m/z=1040.97(p-S1981) were extracted from the LC-MS/MS data and integrated with the Skyline data analysis application[12] using z=2 and an isotope count of 3 (Supplemental Figure S1). The peak identities were manually confirmed by comparing corresponding MS/MS spectra to those obtained from peptide standards. The MS1 intensity ratio (p-S1981/

S1981) for rATM was determined to be 0.44 ± 0.03 (n=3). To adjust for ionization efficiency differences, the MS1 intensity ratio was divided by the MS1 intensity ratio (0.60 ± 0.02) of a synthetic peptide sample that contained equimolar amounts of S1981 andp-S1981. From these data, the molar ratio of pS1981/S1981 in rATM was calculated (0.73), corresponding to 42% of rATM phosphorylated at S1981 [0.73/(1+0.73)].

2.6. Sample Collection

Blood collection and PBMC isolation was performed as reported[5] except that viable PBMCs were counted using the Cellometer K2 cell imager (Nexcelom Bioscience).

Preparation of QC Controls—To prepare PBMC QC controls, 4 CPTs (cat#362761, Becton Dickinson) were collected (four men and four women volunteers; 32 CPTs total). Two CPTs/volunteer were irradiated with 2.0 Gy IR (Shepherd Mark I Model 68 [137Cs] irradiator (J.L.Shepherd & Associates) at a dose rate of 71.1 Rad/m in) and pooled to serve as the “activated” PBMC control. The “basal” control was fashioned from the remaining untreated CPTs. Pellets (1.5×10^6 cells/pellet) were isolated as described above and stored at −70°C.

2.7. Preparation of rATM Calibration Standards

A single-use aliquot of neat rATM was diluted in 2× DTT-modified Laemmli buffer. Three ATM concentrations (0.8, 400, 800 ng/mL), corrected for purity (reported in the COA), were discretely prepared. The 3-point rATM concentration curve captures the upper and lower limits of detection. Inclusion of additional concentrations is constrained by the number of lanes present in commercially-available precast gels. Accordingly, p-S1981-ATM values of 0.34, 168, and 336 ng/mL, respectfully, were assigned from the LC-MS/MS determination (42% of rATM phosphorylated on S1981).

2.8. Immunoblot Assay

The immunoblot procedure was performed as previously published with two exceptions [5]. The sample volume loaded onto the gel lane was 12.5 μL (250,000 cells/lane) and transfer to the membrane was accomplished with constant 100V for 30 minutes.

2.9. Pre-analytical and Analytical Performance Characteristics

Characteristics such as specimen stability, specimen dilutional linearity, near-infrared fluorescence signal quantitation, analytical specificity and multiplexed antibody compatibility have been reported [5].

2.10. rATM Stability

To determine the stability of the rATM calibrator, multiple freeze/thaw cycles were performed. For one freeze/thaw cycle, a rATM aliquot was thawed on ice, placed at RT for 1 hour, then flash-frozen and stored at −70°C overnight. This was repeated three, four, or six times. Each aliquot was prepared at 400 and 800 ng/mL (p-S1981-ATM concentrations of 168 and 336 ng/mL). All samples were measured in duplicate with a three-point standard curve and QC controls. The effect of multiple freeze/thaw cycles on ATM concentration was

evaluated by direct comparison to corresponding concentrations of “fresh” three-point ATM calibration standards frozen and thawed once. Additionally, the reusability of a previously prepared rATM standard (336/800 ng/mL, p-S1981-ATM/pan-ATM) refrozen and stored at −70°C was evaluated. This rATM standard was thawed a second time to create a five-point standard curve for comparison with an identical five-point standard curve generated from a new rATM aliquot, thawed only once. Both curves were run on the same gel.

2.11. Limit of Blank

The limit of blank (LoB) was calculated by adding 3.291 SD to the mean near-infrared fluorescence signals detected for an “ATM-free” sample. Thirty background measurements were taken at 6 different locations (five per location; two above and below the ATM band, with one taken at the level of the ATM band) from three lanes located near either membrane end. The membrane was scanned at 700 nm and 800 nm. Mean values are the average of two immunoblots with 30 replicates/analyte/blot.

2.12. Intra-assay Imprecision

To assess intra-assay random error, basal and 2.0 Gy IR PBMC lysates, from two volunteers, were assayed in sextuplicate or septuplicate. To minimize gel loading position variability, lysates were loaded in an alternating fashion. Additionally, imprecision profiles were charted to visualize the distribution of the within-assay imprecision. The cv of the controls and unknowns, assayed in duplicate, versus their corresponding analyte concentrations or calculated ratios, were gathered from 22 individual immunoblots (n = 148). A second order polynomial was fitted to the data to construct a trendline representing the expected intra-assay error distribution.

2.13. Inter-assay Imprecision

Random inter-assay error was estimated from data accumulated from 22 immunoblots. All samples were run in duplicate containing a three-point calibration curve and QC controls. The inter-assay cv was calculated by dividing the pooled SD by the cumulative mean of duplicates for both QC controls.

2.14. Relative Analytical Accuracy

To evaluate proportional systematic error, spike and recovery studies were conducted. A pooled PBMC lysate was prepared. rATM stock solutions (pan-ATM at 800, 1600, 2400, 3200, and 4000 ng/ml_, and accordingly, p-S1981-ATM at 336, 672, 1008, 1344, and 1680 ng/mL) were prepared in lysis buffer. 10 μL of the ATM stock solution was added into 90 μL of the pooled lysate. For the “spike-free” test sample, 10 μL of lysis buffer was added to 90 μL of the pooled PBMC lysate. The ‘spike-free” test sample was run in quadruplicate with ATM standards, QC controls and the spiked test samples, assayed in duplicate.

2.15. Fit-for-Purpose Validation

To demonstrate the utility of our method, blood was obtained from 41 volunteers (21 men and 20 women). Each volunteer had four CPTs collected during a single venipuncture. Two

CPTs were irradiated (2 Gy) and the remaining CPTs were untreated. PBMCs were isolated and stored.

2.16. Statistical Analysis

Regression analyses, Student's t-tests, second order polynomial trendlines, and descriptive statistics were performed using Excel 2016. Data are presented as mean ± SD. For paired Student's t-tests, $p<0.05$ was considered significant. The Pearson product-moment coefficient (r) measures the linear relationship between two variables on a scatterplot. A coefficient of ±1.0 is perfect; >±0.9 to ±0.99 is considered an excellent relationship. The ratio %p-ATM was calculated as (p-S1981-ATM concentration/pan-ATM concentration) ×100. Analytical bias was calculated as (recovered amount/spiked amount) ×100, where recovered amount = (spiked amount found - mean "spike-free" amount found).

The following analyses used R (version 3.4.3), are 2-sided, and p-value <0.05 is considered significant. Wilcoxon Signed-Rank tests compared treated and untreated samples of the same volunteer as well as between males and females. Spearman correlation coefficients evaluated the correlation between continuous variables. ROC analyses were performed and AUC was calculated with corresponding 95% confidence intervals (CIs, calculated by resampling). Optimal cutoffs to distinguish treated and untreated samples were determined by Youden Index. Non-parametric percentile-based bootstrap 95% CIs for sensitivity, specificity and Youden Index at the optimal cutoffs were provided.

3. Results

3.1. rATM Calibration Standard

To utilize commercially-available rATM as the calibration standard, we determined the percentage of the protein that was phosphorylated on S1981 by MS. rATM was resolved by SDS-PAGE, followed by in-gel trypsin digestion and LC-MS/MS to identify and quantify the intensity of p-S1981 and S1981-specific peptides. Comparing the synthetic peptide intensities provided a measure of the percent of rATM that is phosphorylated at S1981 (42% ± 3%). The rATM calibrator exhibited linearity over a 200-fold range (p-S1981-ATM: 1.68 to 336, pan-ATM: 4 to 800 ng/mL) (Fig. 1; Fig. S2A). Unweighted linear regression analysis yields Pearson product-moment coefficients of 0.99997 and 0.99998 for p-S1981-ATM and pan-ATM, respectively. Additional studies using lower rATM concentrations revealed an overall linearity over a 2000-fold range (lowest concentration 0.4 ng/mL; Fig. S2B).

To determine the stability of the rATM calibrator, multiple freeze/thaw cycles were performed with two different protein amounts. Three freeze/thaw cycles of rATM exhibited a negligible decrease (4% and 6% for p-S1981-ATM and pan-ATM, respectively). However, four and six freeze/thaw cycles showed substantial decreases in p-S1981-ATM (45% and 72%) and pan-ATM (46% and 71%) (Fig. S3A).

Given this result, we compared the signal intensity of a freshly prepared five-point calibration standard with one previously prepared and refrozen. The curves were nearly superimposable suggesting a once-thawed calibrator can be reused without signal loss (Fig. S3B).

3.2. Limit of Blank, Limit of Detection and Limit of Quantitation

Limit of Blank (LoB) was determined to be 0.038 and 0.712 ng/mL for p-S1981-ATM and pan-ATM, respectively. The limit of detection (LoD) was chosen to be the lowest calibration standard level, 0.336 and 0.8 ng/mL for p-S1981-ATM and pan-ATM, respectfully. The limit of quantitation (LoQ) was arbitrarily set to 2.5×LoD.

3.3. Relative Accuracy

To evaluate the accuracy of ATM quantitation, rATM protein was added to a pooled PBMC lysate. The average proportional systematic error detected by spike and recovery testing was acceptably low for both p-S1981-ATM (−3%) and pan-ATM (1%), with recoveries from 95% to 99% and 94% to 114%, respectfully (Table S1).

3.4. Intra-Assay Imprecision

Intra-assay imprecision was determined by analyzing the same PBMC sample in multiple lanes on the same gel. The highest within-assay cv was 7.9% and was associated with a basal pan-ATM concentration of 24.6 ng/10^7 cells. The lowest cv was 0.9% for a p-S1981-ATM value of 17.7 ng/10^7 cells, from a 2.0 Gy IR specimen (Table 1).

3.5. Intra-Assay Imprecision Profiles

To detect intra-assay imprecision, the cv was measured for all 148 samples analyzed in duplicate. A second order polynomial trendline fitted to the within-assay random error of P-S1981-ATM reveals a cv <4% across a range of 0.168 – 309 ng/10^7 cells (Fig. S4). Nevertheless, 10% of the samples (14/148) have a cv >10%<33% for p-S1981-ATM. The pan-ATM intra-assay imprecision expressed a cv consistently <3% for a range of 0.45 – 536.5 ng/10^7 cells. Likewise, for pan-ATM, 5% of measurements (8/148) showed a cv >10%<19%.

3.6. Inter-Assay Imprecision

To demonstrate inter-assay imprecision, we quantified QC samples in 22 individual immunoblots over a 6-month period. Despite the acceptably low intra-assay imprecision (Table 1), a between-assay random error of 148% was observed for p-S1981-ATM expression in the basal QC sample (Table 2). The variation in pan-ATM levels was also highly imprecise. Interestingly, the percentage of ATM protein that was phosphorylated following IR (%p-ATM) had an acceptable cv of 24%. Thus, the variability lies in the blotting *per se*, and is not present in the %p-ATM values.

3.7. Inter-Operator Variability

To investigate the inter-assay imprecision, a second operator performed the assay six times using the same reagents and QC samples. There were minimal differences detected between operators for the average of means of the basal concentration of p-S1981-ATM, and pan-ATM, respectively (Table 2). In the IR exposed QC samples, pan-ATM means were similar (4% difference) while operator B detected somewhat lower concentrations for p-S1981-ATM (39% difference). Similarly, comparing the interoperator variability of %p-ATM, a difference of 11 *%,* and 32%, was observed for the basal and IR exposed PBMC controls,

respectively. Regardless of the quantitative similarities, the high degree of inter-assay imprecision persisted.

3.8. Fit-for-purpose validation: Quantitation of p-S1981 -ATM/pan-ATM in human PBMCs

To establish basal levels of p-S1981-ATM and pan-ATM protein in PBMCs, we obtained blood from 41 volunteers. Blood was mock-irradiated or 2 Gy irradiated. We selected this single radiation dose as it resulted in maximal phosphorylation of S1981 on ATM [3, 4]. Following treatment, PBMCs were isolated and p-S1981-ATM/pan-ATM was analyzed in duplicate. A standard curve (0.8, 400, and 800 ng/mL rATM) was run in duplicate on each immunoblot along with QC samples. We observed a median basal concentration of 2.4 ng p-S1981-ATM/10^7 PBMCs (range: 0.04 - 74.4) and 49.5 ng pan-ATM/10^7 PBMCs (range: 3.9 – 297.3) (Table 3). The range of p-S1981-ATM expression varied by ~370-fold whereas pan-ATM varied by ~76-fold. A weak Pearson product-moment correlation was observed between age and basal p-S1981-ATM, pan-ATM, %p-ATM and activated and %p-ATM (r = 0.296, 0.261, 0.195, and 0.268, respectively). Based on the calculated LoQ (0.42 ng/10^7 cells), three women and one man had basal levels of p-S1981-ATM below quantification. All had quantifiable pan-ATM levels.

3.9. Radiation-induced p-S1981-ATM

The Wilcoxon Rank-Sum test showed no significant sex difference for median basal levels of p-S1981-ATM or pan-ATM. Additionally, no sex differences were observed for pan-ATM levels following DNA damage ($p = 0.1$). However, women showed a 2.6-fold greater median p-S1981-ATM level following exposure to 2 Gy IR than men (44.4 and 16.9 ng/10^7 cells, respectively; $p < 0.01$). This resulted in a significant greater %p-ATM for women (68% versus 49%; $p < 0.01$).

3.10. Receiver-Operating Characteristics

Receiver-operating characteristic (ROC) curves evaluate the diagnostic performance of a test for each measurement. The area under the curve (AUC) quantifies the ability of a test to discriminate normal versus DNA damaged tissues. Both p-S1981-ATM and %p-ATM measurements can detect DNA damaged samples acceptably. The AUC for p-S1981-ATM is 0.936 (95% CI=(0.883, 0.989)) and for %p-ATM is 0.999 (95% CI=(0.996,1)) (Table S2; Fig. S5). The pan-ATM measurement cannot discriminate DNA damaged samples from normal samples (AUC, 0.544; 95% CI=(0.418, 0.67)). Using an optimal cut-off value of 31 % for %p-ATM, sensitivity is 98% and specificity is 100% (Table S2; Fig. 2).

3.11. Radiation-induced p-S139-H2AX

H2AX is one of the many proteins phosphorylated by activated ATM. Previously, we have developed a quasi-quantitative multiplexed immunoblot for detection of γH2AX and pan-H2AX [4, 5]. Attempts to identify a commercially-available source of human recombinant H2AX protein to serve as the reference standard for both γH2AX and pan-H2AX in our assay were unsuccessful. Nonetheless, we analyzed the γH2AX/pan-H2AX ratio in PBMCs irradiated with 2 Gy IR which was normalized to the ratio present in untreated PBMCs. The median H2AX fold induction was 3.08 (range 0.51 – 12.32). As observed previously[4], the

fold activation of H2AX was much lower than ATM (Fig. 3A). Interestingly, H2AX activation did not correlate with ATM activation (p=0.58). Moreover, irradiated PBMCs from males had a slightly greater mean induction of H2AX (4.1-fold) than females (2.7-fold) following 2 Gy IR (Fig. 3B, p=0.042).

4. Discussion

We report the analytical characteristics and fit-for-purpose validation of our novel quantitative dual-labeled immunoblot method that simultaneously measures p-S1981-ATM and pan-ATM in human PBMCs. The accomplishments of this work are: (1) the first reported quantitative measurements of p-S1981-ATM in humans; (2) the introduction of an innovative ratio (%p-ATM) as a novel biomarker of DNA damage; (3) validation of this technique using internal PBMC QC controls; (4) the use of a rATM calibrator to enable the legitimate comparison of data between immunoblots; (5) open and unadulterated reporting of the imprecision of the immunoblot method; and (6) use of commercially available critical reagents making this procedure readily accessible to the scientific community.

The use of PBMCs as a surrogate tissue to assess chemotherapeutic activity of novel molecular agents is logistically and ethically more attractive to oncologists, cancer researchers, and patients than invasive tumor biopsies [13]. However, because of the nature of normal tissue responses, the sample timing may affect the interpretation of the results. Nevertheless, the endpoints observed in human PBMCs may correlate with observations made in the clinic and immune responses to therapies may be directly observed. Clinical trials incorporating this assay as a PD biomarker are ongoing.

Internal assay QC requires obtaining objective evidence indicating performance is reliable and trustworthy between assays [14]. Although most clinical laboratory errors emerge in the pre-analytical and post-analytical phases, 7%-13% of the error transpires during the analytical phase [15]. Therefore, internal QC necessitates the routine measurement of appropriate controls. The source of the QC control should be identical to the unknown samples being examined. All immunoblots evaluated contained a pair of PBMC QC lysates, assayed in duplicate, for a total of four discrete QC values per immunoblot. The expected random error of this method was ascertained from the statistical analysis of QC values obtained from a total of 22 immunoblots. Based upon these error estimates, modern “Westgard Rules” have been established to determine when corrective action should be taken to prevent test failure [16–18].

Presently, a severe paucity of published information exists regarding the imprecision of immunoblotting. A PubMed search using the identifier “Western Blot” returned 311,783 items. The phrase “Western blot imprecision” returned 10. The multi-step process of immunoblotting indisputably introduces error. Our inter-assay data depicts immunoblotting as inherently imprecise [19–21]. A major source of imprecision lies in the transfer of proteins from the precast gel onto the membrane. Our inter-assay random error of >100%, in a Western blot we have been working to standardize over an interval of years, should be alarming to biomedical researchers who use immunoblotting techniques.

Our unexpected finding that there is more DNA damage signaling in PBMCs collected from women than men exposes the limitations of previous assays utilized to detect DNA damage. A commonly used measurement of DNA damage is phosphorylation of histone H2AX on serine 139 (γH2AX) around DSBs as first described by W.M. Bonner [22]. γH2AX foci can be present in the absence of exogenous DNA damage and this may be a consequence of endogenous metabolism that generates reactive oxygen species and replication-associated DSBs. Revet et al concluded that while γH2AX is important during repair of DSBs following γ-radiation, it has little functional importance in DNA repair after exposure to UV, cisplatin, and other crosslinking agents, and the quantity of γH2AX has little correlation to its functional role [23]. γH2AX can appear in a variety of staining patterns besides discrete foci, such as nuclear ring staining and pan-nuclear staining [24, 25]. Detection of γH2AX with our quasi-quantitative assay demonstrated that PBMCs from males had slightly greater H2AX activation than females following 2 Gy IR. However, γH2AX did not correlate with ATM activation and thus, its meaning is unclear. This suggests that another kinase besides ATM may contribute to phosphorylation of H2AX in PBMCs. Several studies have found no sex differences in yH2AXfoci in IR-damaged PBMCs [26, 27]. There is no reason to believe that the number of DSBs induced by IR differs between male and female cells. But our data clearly show that the ATM kinase-dependent DNA damage response induced by 2 Gy IR, ~70 DSBs [28], is increased in women. Additional larger cohort studies are underway to validate our observation. While the current literature is unclear and conflicting with regard to sex-dependent differences in DNA damage response [29], it is reasonable to speculate that cellular responses to IR and DSBs will differ between women and men and this may be manifest as different responses/toxicities in the clinic.

Supplementary Material

Refer to Web version on PubMed Central for supplementary material.

Acknowledgments:

This project used the Hillman Cancer Proteomics Facility and Hillman Pharmacokinetics and Pharmacodynamics Facility that are supported in part by award P30-CA047904 and the UPCI Clinical Translational Research Center that is supported in part by awards UL1RR024153 and UL1TR000005. The authors would like to formally recognize and graciously thank all the many volunteers who kindly participated.

Funding sources: This work was supported by NIH Grants R01 CA204173 and UM1 CA186690-03 (including a biomarker supplement award).

Abbreviations:

ATM	ataxia telangiectasia-mutated kinase
AUC	area under the curve
Bkg	background
COA	certificate of analysis
CPT	cell preparation tube

cv	coefficient of variation
DDR	DNA damage response
DSBs	DNA double-strand breaks
DTT	dithiothreitol
Gy	gray
IR	ionizing radiation
LC-MS/MS	liquid chromatography-tandem mass spectrometry
LoB	Limit of blank
LoD	Limit of detection
LoQ	Limit of quantitation
NIR	near infrared
PBMCs	peripheral blood mononuclear cells
PD	pharmacodynamic
p-S1981-ATM	ATM phosphorylated at serine 1981
%p-ATM	ratio of p-S1981-ATM/pan-ATM
PI	protease inhibitor
PPI	phosphatase inhibitor
PVDF	polyvinylidene fluoride
QA	quality assurance
QC	quality control
rATM	recombinant ataxia telangiectasia-mutated
RFU	relative fluorescent unit
ROC	receiver operating characteristic
RT	room temperature
SD	standard deviation
SDS-PAGE	sodium dodecyl sulfate polyacrylamide gel electrophoresis
SOP	standard operating procedure

References

[1]. Workman P, Challenges of PK/PD measurements in modern drug development, Eur. J. Cancer 38 (2002)2189–2193. [PubMed: 12387843]

[2]. Hoeijmakers JH, DNA damage, aging, and cancer, N. Engl. J. Med 361 (2009) 1475–1485. [PubMed: 19812404]

[3]. Bakkenist CJ, Kastan MB, DNA damage activates ATM through intermolecular autophosphorylation and dimer dissociation, Nature 421 (2003) 499–506. [PubMed: 12556884]

[4]. Bakkenist CJ, Czambel RK, Clump DA, Greenberger JS, Beumer JH, Schmitz JC, Radiation therapy induces the DNA damage response in peripheral blood, Oncotarget 4 (2013) 1143–1148. [PubMed: 23900392]

[5]. Bakkenist CJ, Czambel RK, Hershberger PA, Tawbi H, Beumer JH, Schmitz JC, A quasi-quantitative dual multiplexed immunoblot method to simultaneously analyze ATM and H2AX Phosphorylation in human peripheral blood mononuclear cells, Oncoscience 2 (2015) 542–554. [PubMed: 26097887]

[6]. Bakkenist CJ, Beumer JH, Schmitz JC, ATM serine-1981 phosphorylation is a plausible biomarker, Cell Cycle 14 (2015) 3207–3208. [PubMed: 26517194]

[7]. Wagner JA, Overview of biomarkers and surrogate endpoints in drug development, Dis. Markers 18 (2002) 41–46. [PubMed: 12364809]

[8]. Lee JW, Devanarayan V, Barrett YC, Weiner R, Allinson J, Fountain S, Keller S, Weinryb I, Green M, Duan L, Rogers JA, Millham R, O'Brien PJ, Sailstad J, Khan M, Ray C, Wagner JA, Fit-for-purpose method development and validation for successful biomarker measurement, Pharm. Res 23 (2006) 312–328. [PubMed: 16397743]

[9]. Aguilar HN, Zielnik B, Tracey CN, Mitchell BF, Quantification of rapid Myosin regulatory light chain phosphorylation using high-throughput in-cell Western assays: comparison to Western immunoblots, PLoS One 5 (2010) e9965. [PubMed: 20376358]

[10]. Naskar S, Datta K, Mitra A, Pathak K, Datta R, Bansal T, Sarkar S, Differential and conditional activation of PKC-isoforms dictates cardiac adaptation during physiological to pathological hypertrophy, PLoS One 9 (2014) e104711. [PubMed: 25116170]

[11]. Braganza A, Li J, Zeng X, Yates NA, Dey NB, Andrews J, Clark J, Zamani L, Wang XH, St Croix C, O'Sullivan R, Garcia-Exposito L, Brodsky JL, Sobol RW, UBE3B Is a Calmodulin-regulated, Mitochondrion-associated E3 Ubiquitin Ligase, J. Biol. Chem 292 (2017) 2470–2484. [PubMed: 28003368]

[12]. MacLean B, Tomazela DM, Shulman N, Chambers M, Finney GL, Frewen B, Kern R, Tabb DL, Liebler DC, MacCoss MJ, Skyline: an open source document editor for creating and analyzing targeted proteomics experiments, Bioinformatics 26 (2010) 966–968. [PubMed: 20147306]

[13]. Ang JE, Kaye S, Banerji U, Tissue-based approaches to study pharmacodynamic endpoints in early phase oncology clinical trials, Curr. Drug Targets 13 (2012) 1525–1534. [PubMed: 22974395]

[14]. Kinns H, Pitkin S, Housley D, Freedman DB, Internal quality control: best practice, J. Clin. Pathol 66 (2013) 1027–1032. [PubMed: 24072731]

[15]. Plebani M, The detection and prevention of errors in laboratory medicine, Ann. Clin. Biochem 47 (2010) 101–110. [PubMed: 19952034]

[16]. Rej R, Effect of incubation with Mg2+ on the measurement of alkaline phosphatase activity, Clin. Chem 23 (1977) 1903–1911. [PubMed: 902417]

[17]. Westgard JO, Selecting appropriate quality-control rules, Clin. Chem 40 (1994) 499–501. [PubMed: 8131294]

[18]. Westgard JO, Westgard SA, Quality control review: implementing a scientifically based quality control system, Ann. Clin. Biochem 53 (2016) 32–50. [PubMed: 26150675]

[19]. Koller A, Watzig H, Precision and variance components in quantitative gel electrophoresis, Electrophoresis 26 (2005) 2470–2475. [PubMed: 15924365]

[20]. Schroder S, Zhang H, Yeung ES, Jansch L, Zabel C, Watzig H, Quantitative gel electrophoresis: sources of variation, J. Proteome Res. 7 (2008) 1226–1234. [PubMed: 18220338]

[21]. Schroder S, Brandmuller A, Deng X, Ahmed A, Watzig H, Improving precision in gel electrophoresis by stepwisely decreasing variance components, J. Pharm. Biomed. Anal 50 (2009) 320–327. [PubMed: 19501482]

[22]. Rogakou EP, Pilch DR, Orr AH, Ivanova VS, Bonner WM, DNA double-stranded breaks induce histone H2AX phosphorylation on serine 139, J. Biol. Chem 273 (1998) 5858–5868. [PubMed: 9488723]

[23]. Revet I, Feeney L, Bruguera S, Wilson W, Dong TK, Oh DH, Dankort D, Cleaver JE, Functional relevance of the histone gammaH2Ax in the response to DNA damaging agents, Proc. Natl. Acad. Sci. U. S. A 108 (2011) 8663–8667. [PubMed: 21555580]

[24]. White JS, Yue N, Hu J, Bakkenist CJ, The ATM kinase signaling induced by the low-energy beta-particles emitted by (33)P is essential for the suppression of chromosome aberrations and is greater than that induced by the energetic beta-particles emitted by (32)P, Mutat Res 708 (2011) 28–36. [PubMed: 21315088]

[25]. Solier S, Pommier Y, The nuclear gamma-H2AX apoptotic ring: implications for cancers and autoimmune diseases, Cell. Mol. Life Sci. 71 (2014) 2289–2297. [PubMed: 24448903]

[26]. Garm C, Moreno-Villanueva M, Burkle A, Petersen I, Bohr VA, Christensen K, Stevnsner T, Age and gender effects on DNA strand break repair in peripheral blood mononuclear cells, Aging Cell 12 (2013) 58–66. [PubMed: 23088435]

[27]. Sharma PM, Ponnaiya B, Taveras M, Shuryak I, Turner H, Brenner DJ, High throughput measurement of gammaH2AX DSB repair kinetics in a healthy human population, PLoS One 10 (2015) e0121083. [PubMed: 25794041]

[28]. Falk M, Lukasova E, Kozubek S, Higher-order chromatin structure in DSB induction, repair and misrepair, Mutat. Res 704 (2010) 88–100. [PubMed: 20144732]

[29]. Borgmann K, Dikomey E, Petersen C, Feyer P, Hoeller U, Sex-specific aspects of tumor therapy, Radiat. Environ. Biophys 48 (2009) 115–124. [PubMed: 19242712]

Highlights

- First reported quantitative measurements of p-S1981-ATM in humans
- Introduction of an innovative ratio (%p-ATM) as a novel biomarker of DNA damage
- Validation of our p-ATM assay using internal PBMC QC controls
- Use of a rATM calibrator to enable comparison between immunoblots
- Use of commercially available reagents making our p-ATM assay readily accessible

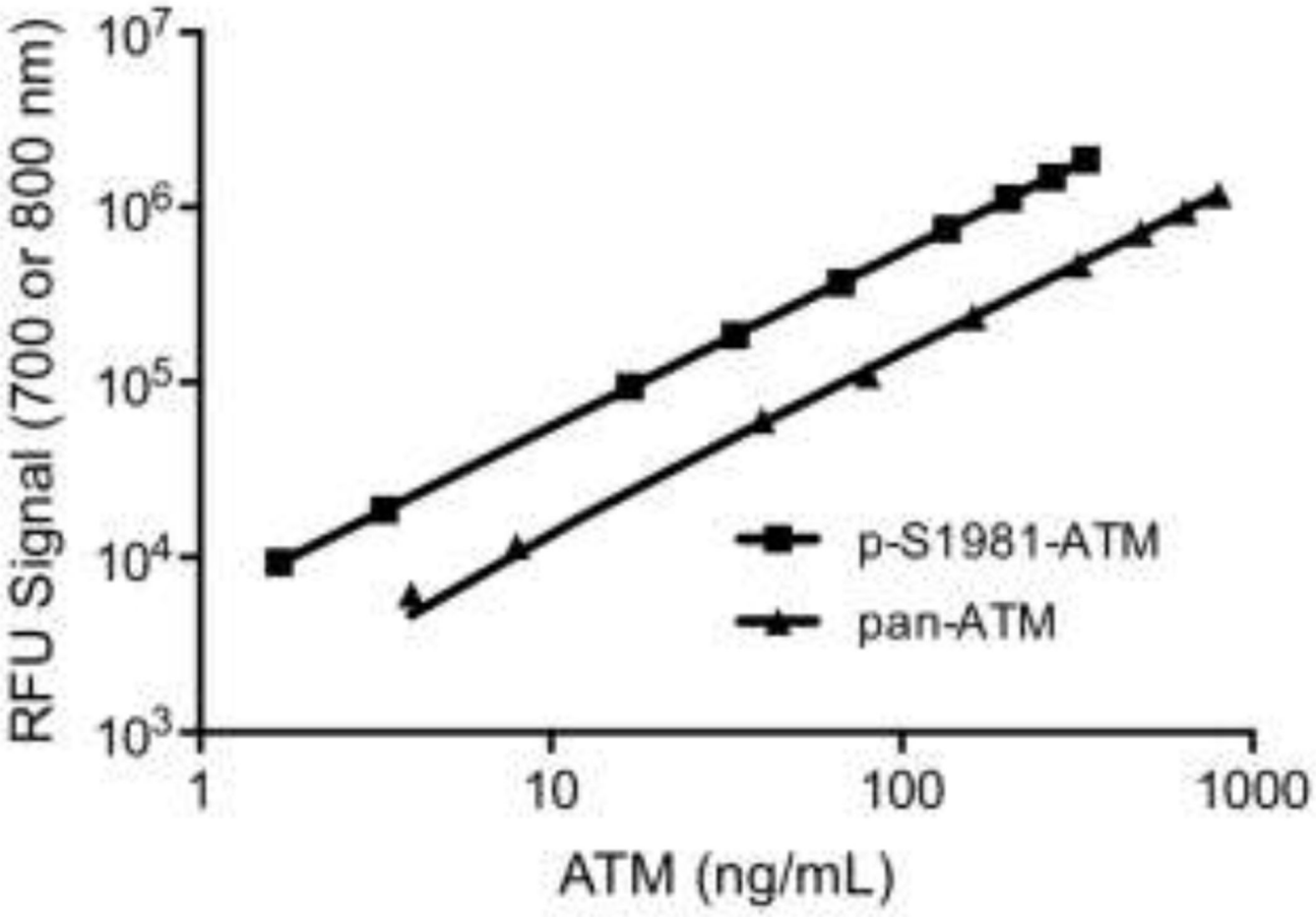

Fig. 1.

Dilutional linearity. rATM protein was electrophoresed on SDS-PAGE (4 to 800 ng/mL) and p-S1981-ATM and pan-ATM protein was detected by immunoblot analysis.

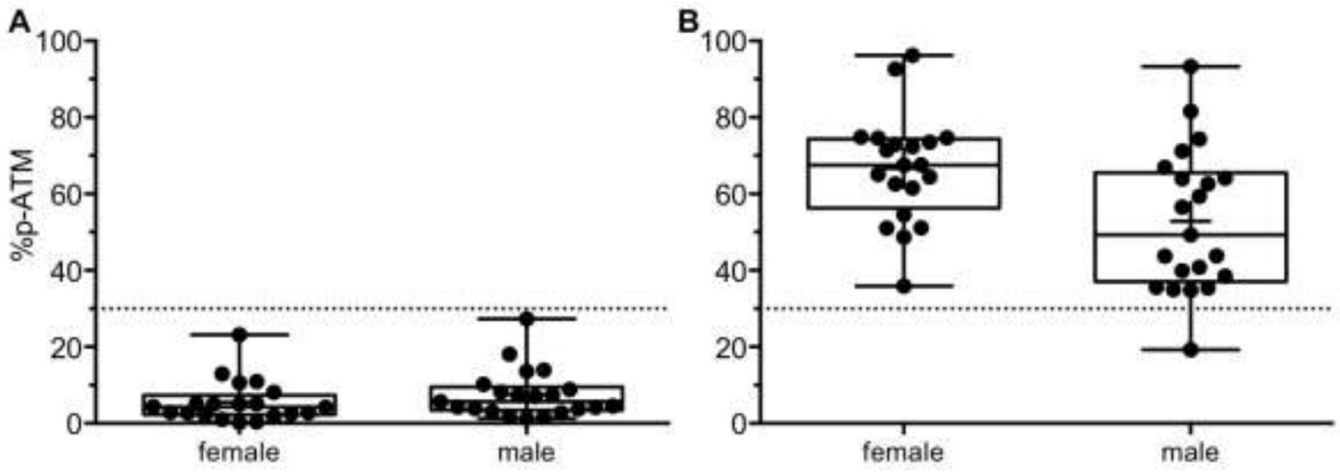

Fig. 2.

Diagnostic accuracy. %p-ATM values for basal (A) and IR-treated PBMCs (B). The dotted lines represent a cut-off value for %p-ATM.

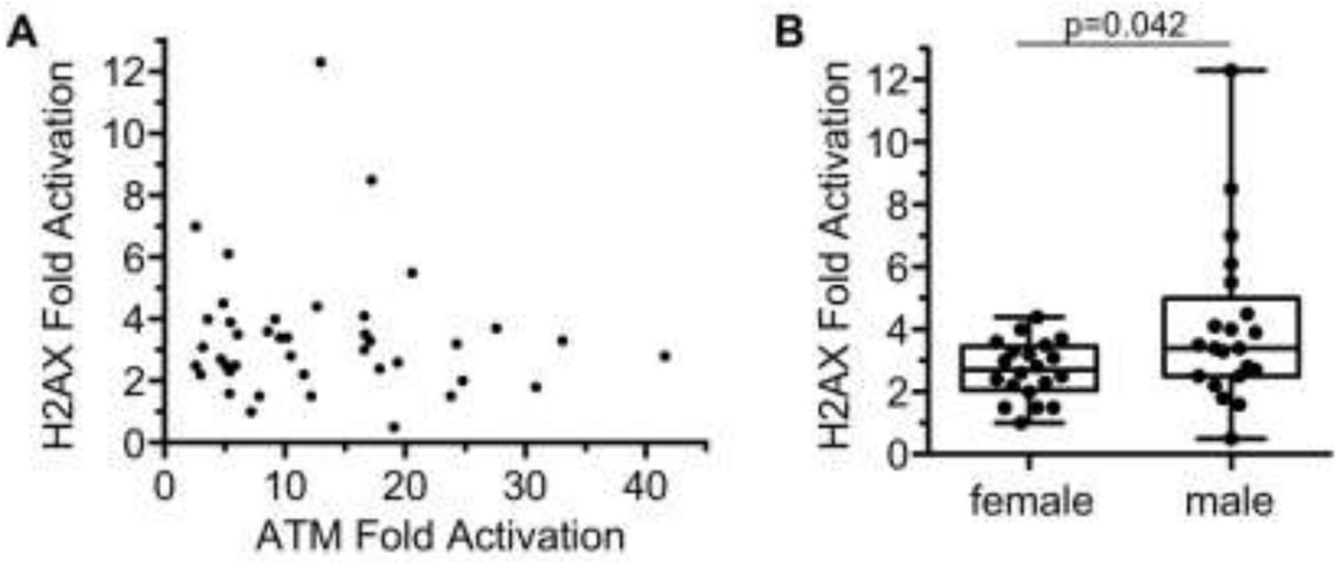

Fig. 3.

H2AX activation in human PBMCs. (A) Comparison of H2AX and ATM activation in 41 volunteers following 2 Gy IR (Spearman correlation coefficient $\rho = -0.09$, p-value=0.58). (B) H2AX activation in females versus males ($p = 0.042$).

Table 1.

Intra-assay imprecision

Sample ID*	Analyte	mean (ng/10_7 cells)	cv%	mean %p-ATM	cv%
Basal A	p-S1981-ATM	3.42 ± 0.11	3.3	13.9 ± 1.0	7.1
	pan-ATM	24.60 ± 1.90	7.9		
2 Gy IR A	p-S1981-ATM	17.70 ± 0.16	0.9	36.3 ± 2.3	6.4
	pan-ATM	48.90 ± 3.40	6.9		
Basal B	p-S1981-ATM	3.85 ± 0.09	2.4	8.5 ± 0.2	2.2
	pan-ATM	45.40 ± 0.70	1.1		
2 Gy IR B	p-S1981-ATM	6.97 ± 0.07	1.1	65.9 ± 1.9	2.8
	pan-ATM	10.06 ± 0.30	2.7		

Values represent the mean ± S.D.

*For subject A, n = 7. For subject B, n = 6.

Table 2.

Inter-assay and inter-operator imprecision

QC Sample ID	Analyte	mean (ng/10^7 cells)	cv%	mean %p-ATM	cv%
Operator A*					
Basal Control	P-S1981-ATM	8.0 ± 11.8	148	10.3 ± 10.0	97
	pan-ATM	66.3 ± 64.5	97		
2 Gy IR Control	P-S1981-ATM	56.1 ± 58.4	104	76.4 ± 18.7	**24**
	pan-ATM	67.3 ± 63.7	95		
Operator B					
Basal Control	P-S1981-ATM	7.6 ± 7.8	103	15.4 ± 20.0	130
	pan-ATM	58.3 ± 22.8	39		
2 Gy IR Control	P-S1981-ATM	37.9 ± 42.6	112	60.0 ± 39.0	65
	pan-ATM	69.9 ± 56.4	81		

*Operator A performed 22 separate assays. Operator B performed 6 separate assays.

Values represent the mean ± S.D.

Table 3.

ATM protein level in human PBMC

Treatment	All subjects median	All subjects range	Female median	Female range	Male median	Male range	p*
Basal P-S1981-ATM (ng/10^7 cells)	2.43	0.04 - 74.38	1.3	0.04 - 32.4	3.12	0.08 - 74.38	0.33
pan-ATM (ng/10^7 cells)	49.46	3.89 - 297.34	47.56	3.89 - 297.34	49.46	6.31 - 272.11	0.85
%p-ATM	4%	0 - 27	4%	0 - 23	6%	1 - 27	0.22
2 Gy IR P-S1981-ATM (ng/10^7 cells)	29.82	5.99 - 301.94	44.44	7.46 - 301.94	16.85	5.99 - 220.6	0.0099
pan-ATM (ng/10^7 cells)	55.71	15.31 - 379.68	73.23	15.31 - 379.68	50.17	15.84 - 270.39	0.1
%p-ATM	63%	19 - 96	68%	36 - 96	49%	19 - 93	0.0077

*Wilcoxon Rank-Sum test p-value comparing female and male values.